Journal of Alloys and Compounds 513 (2012) 474–480

Contents lists available at SciVerse ScienceDirect

Journal of Alloys and Compounds

journal homepage: www.elsevier.com/locate/jallcom

Hydrothermal synthesis and luminescence properties of $GdVO_4:Ln^{3+}$ (Ln = Eu, Sm, Dy) phosphors

Shen Tang, Miaoliang Huang*, Jiangli Wang, Fuda Yu, Guanglu Shang, Jihuai Wu

Institute of Material Physical Chemistry, Huaqiao University, The Key Laboratory for Functional Materials of Fujian Higher Education, Quanzhou, Fujian 362021, China

ARTICLE INFO

Article history:
Received 22 July 2011
Received in revised form 28 October 2011
Accepted 28 October 2011
Available online 7 November 2011

Keywords:
$GdVO_4$
Hydrothermal synthesis
Photoluminescence
Rare-earth ions

ABSTRACT

$GdVO_4:Eu^{3+}$ microcrystals and nanocrystals with different morphologies were successfully synthesized via a simple hydrothermal method in a wide range of pH value, and characterized by X-ray powder diffraction (XRD), scanning electron microscopy (SEM), X-ray energy dispersion spectrum (EDS), transmission electron microscopy (TEM) and photoluminescence (PL) spectrometer. The experimental results indicate that the morphologies and photoluminescence properties of $GdVO_4:Eu^{3+}$ crystals have a strong dependence on the pH values of the solution. Additionally, Dy^{3+}/Sm^{3+} doped $GdVO_4$ were synthesized by hydrothermal method, their luminescent properties were performed. The effects of annealing temperature, rare ions (Eu^{3+}, Sm^{3+} and Dy^{3+}) doping concentration on the photoluminescence emission intensity were also investigated. The $GdVO_4:Ln^{3+}$ (Ln = Eu, Sm, Dy) phosphors show their characteristic emission under ultraviolet excitation due to the efficient energy transfer from VO_4^{3-} group to rare earth ions.

1. Introduction

Rare-earth ions doped rare earth vanadate compounds as phosphors, which can emit various colors light owing to the high luminescence quantum yields originating from the f–f transition have been widely studied [1–8]. Among these phosphors, $YVO_4:Eu^{3+}$ and $GdVO_4:Eu^{3+}$ as red phosphors have attracted a considerable attention because of their integration of good thermal properties, chemical stability and high photoluminescence quantum yield, which makes them had a promising application in color television, field emission displays (FEDs) [9,10], cathode ray tubes (CRTs) [11], light emitting diodes (LED) [12] and plasma display panels (PDPs) [13,14]. Compared to $YVO_4:Eu^{3+}$, $GdVO_4:Eu^{3+}$ has better temperature properties and the intensity of the luminescence increases rapidly with the temperature rises, which makes it can be applied in high temperature environments [15]. The previous investigation results indicated that the luminescence properties of the phosphors depended on their sizes and morphologies [16,17], therefore, the controllable preparation of the size, microstructure and morphology of the phosphor have been paid much attention. Recently, $GdVO_4$ with different morphologies such as nanowires, nanorods, nanofibers and nanoparticles have been reported [5,18–22].

In recent years, much attention has been paid to the synthesis and characterization of nanomaterials due to their interesting physical and chemical properties, which mainly come from the quantum-size effect in nano-system and high surface/volume ratio compared to bulk counterparts [7]. Besides, with the recent development of displays towards the high quality, efficiency and miniaturization, the preparation of nanoparticles to meet the requirement of the host of the phosphors with decreasing size and narrow size distribution is necessary [23,24]. Beyond that, large phosphor particles are more likely to be prone to poor adhesion to the substrate and loss of coating. As well known, different synthesis methods have important effect on material microstructure, morphology and physical properties. Up to now, several synthetic routes have been developed to prepare rare-earth ions doped $GdVO_4$. For instance, solid-state reaction [14], hydro/solvothermal method [2,18,19], in situ co-precipitation reaction [25,26], sol–gel process [27] and electrospinning technology [5]. Among the above synthesis techniques, hydrothermal method is one of the most promising solution chemical methods due to its advantages, such as the powders prepared through hydrothermal route have high purity, narrow particle size distribution and precise composition. Besides, hydrothermal conditions are easily controlled. In the hydrothermal process, the pH value of the solution plays a great part in modifying the morphology, phase and size of the products. Chen et al. have synthesized $YVO_4:Eu^{3+}$ nanocrystalline with different morphologies by adjusting the pH value of the solution, and pointed out the photoluminescence properties changed with different morphologies [17]. Wang et al. have also investigated the influence of pH values (7–11) in the solution on the morphology and PL properties of the $YVO_4:Eu^{3+}$ [23]. Calderón-Villajos et al. have synthesized Tm^{3+}-doped $GdVO_4$ with various morphologies from

* Corresponding author. Tel.: +86 0595 22690582.
E-mail address: huangml@hqu.edu.cn (M. Huang).

0925-8388/$ – see front matter © 2011 Elsevier B.V. All rights reserved.
doi:10.1016/j.jallcom.2011.10.093

a specific combination of conditions (regents, pH, reaction time) in the template-free hydrothermal synthetic procedure [28]. So one can easily control the morphology and size of the powders through the hydrothermal process via adjusting the source of species, pH value of the solution, reaction temperature and time.

In this work, we synthesized $GdVO_4:Ln^{3+}$ (Ln = Eu, Sm, Dy) phosphors by a simple hydrothermal method using $NaVO_3$ as vanadium source, and the photoluminescence properties of as-prepared samples were performed. The effects of pH, annealing temperature, and ions doping concentration on the photoluminescence properties were also investigated.

2. Experimental

2.1. Chemicals

Gd_2O_3 (4N), Eu_2O_3 (4N), Dy_2O_3 (3N), Sm_2O_3 (3N) and $NaVO_3$ (AR) were purchased from Shanghai Chemical Reagent Company, China. Ammonia (25 wt%, AR) and HNO_3 (AR) were obtained from Guangdong Shantou Xilong Chemical Company, China. All reagents were used without any further purification. $Ga(NO_3)_3$ stock solution of 0.1 M was prepared by dissolving the Gd_2O_3 in dilute HNO_3 solution (2 M) under continuous stirring and the residual HNO_3 was removed by elevated temperature. Other rare earth nitrate stock solutions of 0.02 M were prepared by the same method.

2.2. Preparation of $GdVO_4:Ln^{3+}$ (Ln = Eu, Sm, Dy) powders

$GdVO_4:Eu^{3+}$ powders were prepared by a simple hydrothermal method. The typical procedures were as follows: 19 ml of 0.1 M aqueous solution of $Gd(NO_3)_3$ was mixed with 5 ml $Eu(NO_3)_3$ solution (0.02 M) under continuous stirring to obtain a homogeneous solution with a 95:5 of the molar ratio of Gd^{3+}/Eu^{3+}. $NaVO_3$ (0.002 mol) was dissolved in 45 ml of distilled water, subsequently was added dropwise into the above mixed solution under constant stirring. In order to adjust pH value, 25 wt% of ammonia solution or HNO_3 solution (2 M) was dropped into the above mixture under vigorous stirring. After stirring for 20 min, 70 ml of the well-stirred solution was poured into a 100 ml Teflon-lined stainless steel autoclave and heated at 180 °C for 24 h. After that, the autoclave was naturally cooled down to the room temperature. The as-synthesized precipitate was filtered, washed with distilled water and ethanol several times, and then dried at 80 °C in the air. The synthetic procedures of $GdVO_4:Sm^{3+}$ or $GdVO_4:Dy^{3+}$ phosphors were prepared as the same with $GdVO_4:Eu^{3+}$ sample by replacing $Eu(NO_3)_3$ with $Sm(NO_3)_3$ or $Dy(NO_3)_3$.

2.3. Characterization

Powder X-ray diffraction (XRD) patterns were obtained by X-ray diffractometer (XRD, PANALYTICAL, X'Pert PRO, Cu Kα, 40 mA, λ = 0.15406 nm). The morphology and particle size of the as-synthesized products were observed by field emission scanning electron microscopy (FESEM, HITACHI S-4800) and transmission electron microscopy (TEM, HITACHI H-7650). The element analyses of the samples were performed by X-ray energy dispersion spectrum (EDS, Oxford INCA). Edinburgh FLS920 fluorescence spectrometer equipped with 450 W Xe lamp was used to measure the photoluminescence properties of the samples. All the measurements were performed at room temperature.

3. Results and discussion

3.1. Phase, structure and morphology

The XRD patterns of the $GdVO_4:Eu^{3+}$ powders prepared by hydrothermal treatment at 180 °C for 24 h with different pH values are shown in Fig. 1. It is found that all the peaks can be indexed to pure $GdVO_4$, which has a zirconia-type tetragonal structure with the $I4_1/amd$ space group (JCPDS Card no. 86-0996). The diffraction intensities of the samples decrease evidently with the pH value increasing. This phenomenon can be explained as the nanoparticles caused the diffraction peaks broad (see the next SEM and TEM part). No traces of other phases could be detected from the XRD patterns, so small amount of Eu^{3+}-doping does not affect the tetragonal zircon structure of $GdVO_4$. The average particle size of the nanocrystals can be estimated using the Scherrer equation: $D = K\lambda/\beta\cos\theta$. The strongest peak (2 0 0) was used to calculate the average crystallite size of $GdVO_4:Eu^{3+}$ nanocrystals prepared at pHs 4.2, 7.2, 9.3 and 11.1. The mean particle size could be calculated to

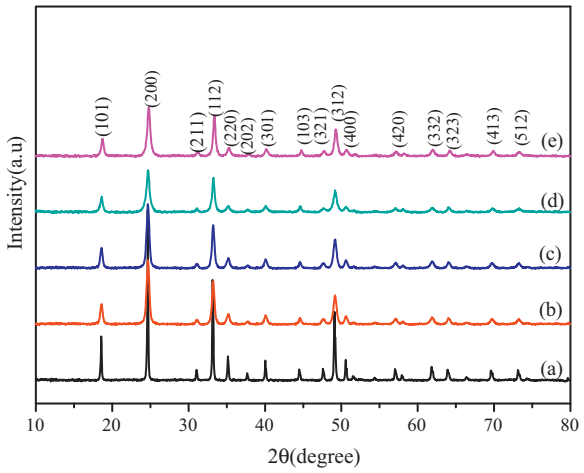

Fig. 1. XRD patterns of $GdVO_4:Eu^{3+}$ powders synthesized at 180 °C for 24 h with different pH values: (a) 2.0, (b) 4.2, (c) 7.2, (d) 9.3, (e) 11.1.

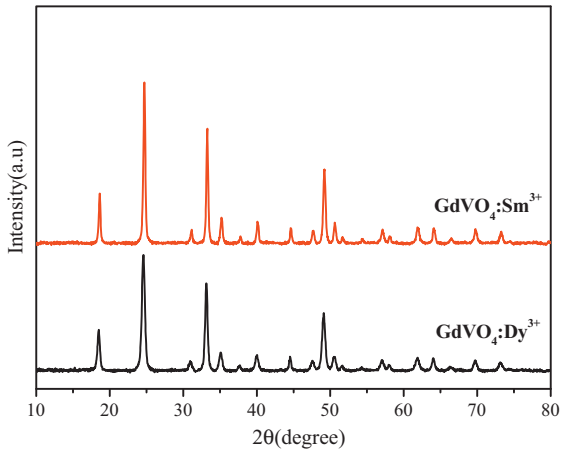

Fig. 2. XRD patterns of $GdVO_4:Ln^{3+}$ (Ln = Dy, Sm) powders synthesized at 180 °C for 24 h with pH value of 7.2.

be 21.6, 32.3, 18.4 and 19.7 nm, respectively. The calculated results are close to those observed from TEM images (seen in Fig. 3C–F).

The XRD patterns of $GdVO_4:Ln^{3+}$ (Ln = Dy, Sm) powders prepared by hydrothermal treatment at 180 °C for 24 h at pH 7.2 are displayed in Fig. 2. All the peaks can be indexed to pure $GdVO_4$ with the cell parameters $a = 7.2122$ Å and $c = 6.3460$ Å (JCPDS Card no. 86-0996). It can be seen that the diffraction peaks of the samples are sharp and narrow, which means that the $GdVO_4:Ln^{3+}$ (Ln = Dy, Sm) phosphors with high crystallinity can be obtained at relatively low hydrothermal temperature (180 °C). This is important for phosphors, because higher crystallinity generally means less defects and stronger luminescence. The calculated unit-cell parameters of the samples are summarized in Table 1. Compared with bulk $GdVO_4$, the lattice constants are elongated a little by the introduction of Eu^{3+} or Sm^{3+} ions, but for the doping of Dy^{3+} ions the lattice constants are shortened a little, indicating that the rare earth ions have doped into the lattices of the $GdVO_4$ host. That is because the ionic radius of the Eu^{3+} (0.947 Å) and Sm^{3+} (0.964 Å) ions is bigger than that of Gd^{3+} ion (0.938 Å), while the ionic radius of Dy^{3+} (0.912 Å) ion is smaller than that of Gd^{3+} ion. The color of the samples synthesized at different pH values is different. The color of $GdVO_4:Eu^{3+}$ powders synthesized at pH 2.0 is deep yellow, pale yellow at pHs 4.2 and 7.2. The white powders are obtained when the pH value increased to 9.3 and 11.1. $GdVO_4:Sm^{3+}/Dy^{3+}$ powders synthesized

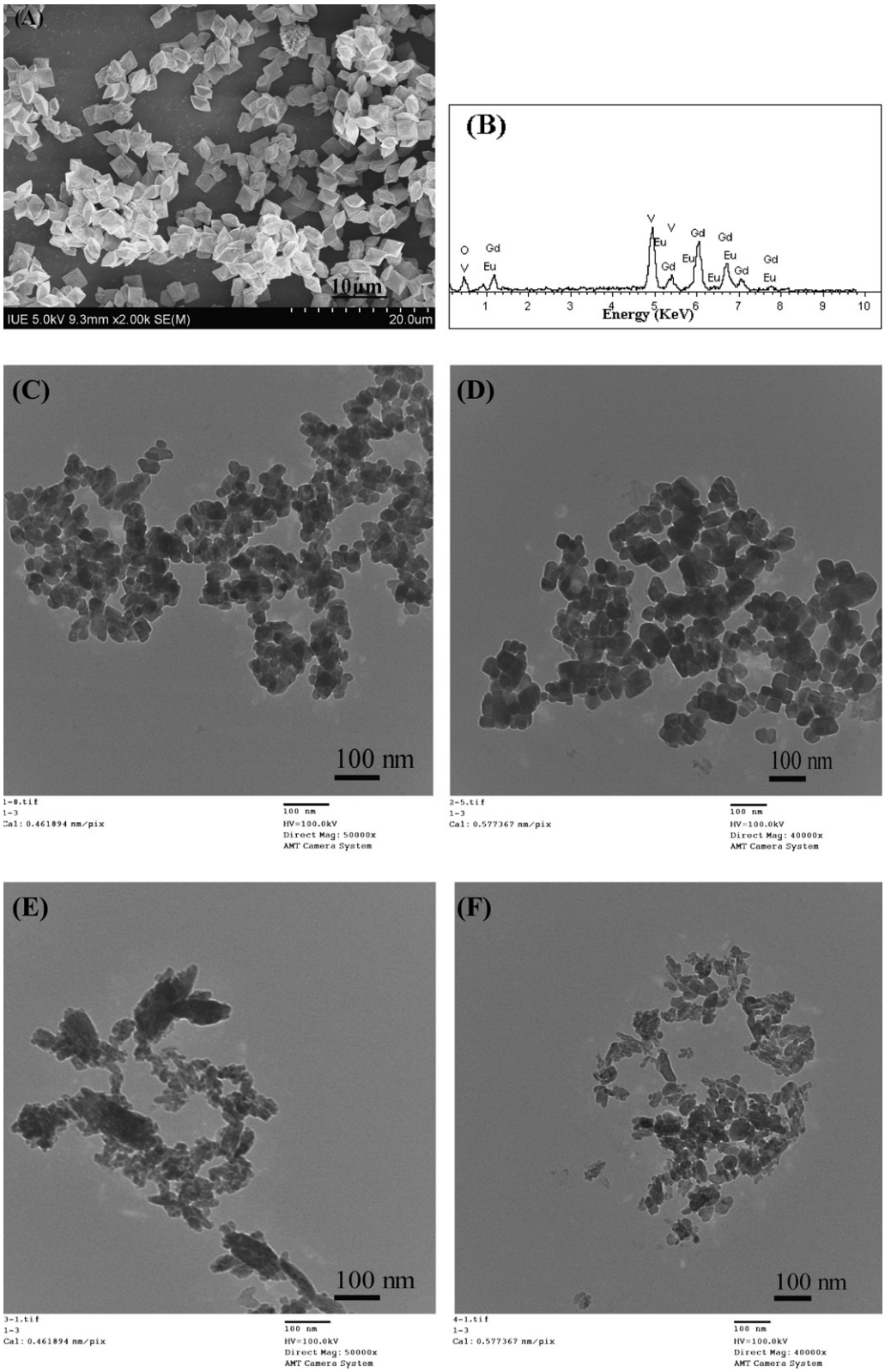

Fig. 3. (A) SEM, (C–F) TEM images for the as-synthesized $GdVO_4$:Eu^{3+} at different pH values: (A) 2.0, (C) 4.2, (D) 7.2, (E) 9.3, (F) 11.1, (B) EDS spectrum of $GdVO_4$:Eu^{3+} prepared at pH 7.2.

at pHs 7.2 and 11.1 are pale yellow and white, respectively, and same color as $GdVO_4$:Eu^{3+} powders.

The EDS spectrum, SEM and TEM micrographs of the $GdVO_4$:Eu^{3+} powders prepared at 180 °C for 24 h with different pH values are illustrated in Fig. 3. It can be seen that the pH value of the reaction solution plays an important role in controlling the morphologies of the final products. The SEM image (Fig. 3A) reveals that the $GdVO_4$:Eu^{3+} microcrystals synthesized at pH 2.0 are composed of relatively uniform rhombic particles with edge length in the range of 1.5–2 μm. With increasing the pH value to 4.2, the

Table 1
Unit-cell parameters and the deviations for the as-prepared $GdVO_4:Eu^{3+}$, $GdVO_4:Dy^{3+}$ and $GdVO_4:Sm^{3+}$ nanocrystals synthesized at 180 °C for 24 h at pH 7.2.

Samples	*a*, *b* (Å)/deviations	*c* (Å)/deviations	*c*/*a*	Vol (Å^3)/deviations
JCPDS 86-0996	7.2122	6.3460	0.8799	330.09
$GdVO_4:Eu^{3+}$	7.2227/0.0105	6.3572/0.0112	0.8802/0.0003	331.64/1.55
$GdVO_4:Sm^{3+}$	7.2428/0.0306	6.3884/0.0424	0.8820/0.0021	335.13/5.04
$GdVO_4:Dy^{3+}$	7.1978/0.0144	6.3409/0.0051	0.8809/0.0010	328.51/1.58

morphology of the $GdVO_4:Eu^{3+}$ changed evidently (shown in Fig. 3C), the spherical and cubic $GdVO_4:Eu^{3+}$ nanoparticles with the size about 20 nm were obtained. Fig. 3D shows the TEM image of the $GdVO_4:Eu^{3+}$ powder prepared at pH 7.2. It can be found that the morphologies of the as-prepared $GdVO_4:Eu^{3+}$ do not change much, only the particle size become bigger (about 30 nm) compared to the sample prepared at pH 4.2. When the pH value was adjusted to 9.3, the morphologies of the products transferred into irregular short nanorods (Fig. 3E). The $GdVO_4:Eu^{3+}$ crystals synthesized at pH 11.1 are also composed of irregular short nanorods, shown in Fig. 3F, but the particle size is bigger and the crystallinity is better compared with the sample prepared at pH 9.3. As a result, it can be concluded that the morphology and particle size of $GdVO_4:Eu^{3+}$ phosphor can be manipulated by adjusting the pH value of the hydrothermal solution. Fig. 3B shows the energy-dispersive X-ray spectrum (EDS) analysis of $GdVO_4:Eu^{3+}$ prepared at pH 7.2. The EDS spectrum confirms the existence of gadolinium (Gd), vanadium (V), oxygen (O) and europium (Eu) in the sample. No other elements can be detected from the EDS spectrum, which can effectively support the XRD result (Fig. 1c) of the as-prepared sample.

3.2. Photoluminescence (PL) properties

The PL properties of the as-synthesized $GdVO_4:Ln^{3+}$ (Ln = Eu, Sm, Dy) phosphors were characterized by the PL excitation and emission spectrum. Fig. 4 shows the excitation and emission spectra of the $GdVO_4:Eu^{3+}$ crystals prepared at 180 °C for 24 h at pH 7.2. The excitation spectrum monitored at 618 nm consists of a broad absorption band with a maximum at 313 nm in the range of 250–350 nm and several weak lines in the longer wavelength region (360–500 nm). The strong absorption band can be assigned to the charge transfer from the oxygen ligands to the central vanadium atom inside the VO_4^{3-} groups. According to the standpoint of molecular orbital theory, it corresponds to electric or magnetic dipole-allowed transitions from the $^1A_2$ ($^1T_1$) ground state to ^1E ($^1T_2$) and $^1A_1$ (^1E) excited states of the VO_4^{3-} ion [29,30]. The weak lines are attributed to the f–f transition within the $4f^6$ configuration of the Eu^{3+} ions, but it is very weak with respect to that of the VO_4^{3-} groups. This phenomenon can illustrate that the excitation of the Eu^{3+} ions is mainly through the energy transfer from VO_4^{3-} groups to the Eu^{3+} ions [8].

The PL emission spectrum of the $GdVO_4:Eu^{3+}$ nanoparticles synthesized at pH 7.2 is shown in the right side of Fig. 4. The emission spectrum is composed of several sharp lines ranging from 500 to 750 nm, which is ascribed to the $^5D_0 \rightarrow {}^7F_J$ ($J = 1, 2, 3, 4$) transitions of the Eu^{3+} ion. The emission band around 593 nm can be assigned to the $^5D_0 \rightarrow {}^7F_1$ magnetic dipole transition, and the emission peaks located at about 614 and 618 nm could be ascribed to the transition from $^5D_0$ level to $^7F_2$ energy level, which is an electric–dipole allowed transition and hypersensitive to the environment. The peak located at 698 nm can be assigned to $^5D_0$ level transfer to $^7F_4$ energy level. It can be observed that the peaks from $^5D_0 \rightarrow {}^7F_2$ are stronger than that from $^5D_0 \rightarrow {}^7F_1$ which means that the Eu^{3+} ions locate at low-symmetry local sites without an inversion center (D_{2d} symmetry) [18,30]. Furthermore, it is noticed that there is no emission from the VO_4^{3-} groups, indicating that the energy transfer from the VO_4^{3-} groups to the Eu^{3+} ions is very efficient.

Fig. 5 shows the excitation and emission spectra of the $GdVO_4:Eu^{3+}$ crystals prepared at 180 °C for 24 h with different pH values. The excitation spectrum (Fig. 5, left) monitored at 618 nm with similar shape for the products obtained at different pH values except the excitation intensities different. From Fig. 5, it can be clearly seen that the PL intensity decreases dramatically when the pH value adjusted to 9.3. This phenomenon can be explained by two aspects: (1) from the above XRD results (Fig. 1), it can be concluded that the crystallinity of the $GdVO_4:Eu^{3+}$ synthesized at pH 9.3 is the worst among these samples, so more defects are existed in the crystal which leads to the luminescent intensity decreasing. (2) From the TEM observation, the particle size of the sample prepared at pH 9.3 is smaller than other samples, so more hydroxyl groups can be absorbed on the surface due to the larger surface

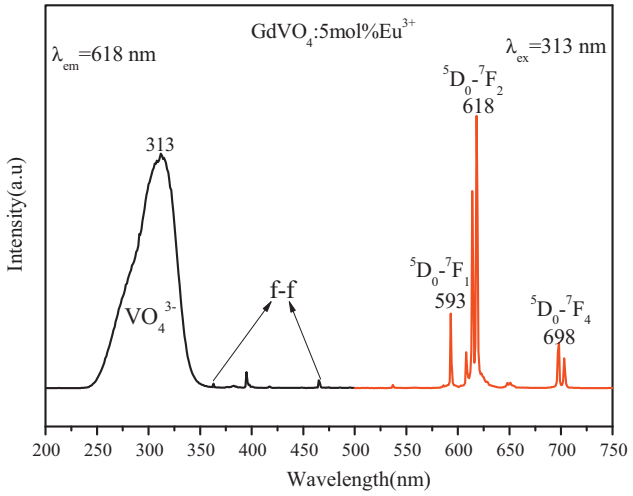

Fig. 4. Excitation and emission spectra of $GdVO_4:Eu^{3+}$ synthesized at 180 °C for 24 h with pH value of 7.2.

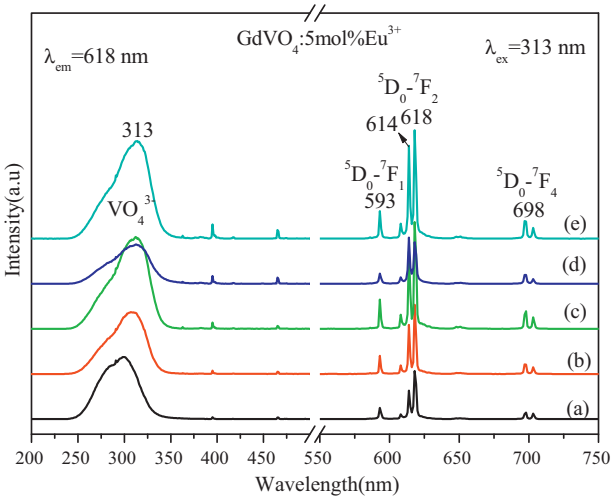

Fig. 5. Excitation and emission spectra of $GdVO_4:Eu^{3+}$ synthesized at 180 °C for 24 h with different pH values: (a) 2, (b) 4.2, (c) 7.2, (d) 9.3, (e) 11.1.

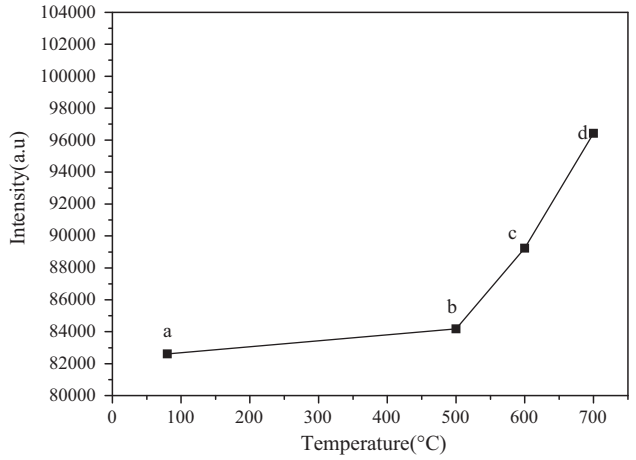

Fig. 6. The photoluminescence emission intensity of $GdVO_4$:Eu^{3+} ($^5D_0 \rightarrow {}^7F_2$) sample annealed at different calcination temperatures for 2 h.

area. It is well known that the hydroxyl groups were to be very efficient quenchers of the luminescence of the lanthanide elements through multiphonon relaxation [23]. The luminescence intensity of the rhombus-like powders is weaker than the samples prepared at pHs 4.2, 7.2 and 11.1 owing to large size and shapes lead to the higher scatting of light [31]. Furthermore, it can be observed that the position of the predominant peak of the sample synthesized at pH 9.2 is changed to 614 nm in comparison with that of the samples synthesized at pHs 1, 4.2, 7.2 and 11.1 respectively from the emission spectra (Fig. 5, right). These irregular short nanorods possess larger surface area and high surface energy, which result in the higher degree of disorder and corresponding lower symmetry of crystal fields around Eu^{3+} ions. It is well known that the $^5D_0 \rightarrow {}^7F_2$ transition is very sensitive to structure change and environment effects. The difference of $^5D_0 \rightarrow {}^7F_2$ emission peak in relative intensity and positions were due to the difference of the effects of the crystal field perturbation on the individual f–f transition. Based on the above understanding, the position of the predominant peak is associated with microstructure and crystallinity [17,23,32].

In order to understand the effect of calcination temperatures on the photoluminescence property, the $GdVO_4$:Eu^{3+} phosphor prepared at pH 7.2 was annealed at different calcination temperatures for 2 h. Fig. 6 shows the emission intensities of the $GdVO_4$:Eu^{3+} phosphor annealed at different calcination temperatures. With the increase of annealing temperatures, the emission intensity ($^5D_0 \rightarrow {}^7F_2$) increased, which can be ascribed to the following two reasons. Firstly, the calcination progress can improve the crystallization of the sample and decrease the concentration of defect [3,5,9,15,17,33–35]. Secondly, the absorbed water or hydroxyl groups on the surface of the as-prepared samples can be removed through the calcination progress [23,34].

The excitation and emission spectra of Sm^{3+} and Dy^{3+} doped $GdVO_4$ are shown in Fig. 7A and B respectively. As for $GdVO_4$:Sm^{3+}, the excitation spectrum (Fig. 7A, left) monitored at 602 nm consists of a broad band with a maximum at 316 nm assigned to $VO_4{}^{3-}$ absorption. Upon 312 nm excitation, the characteristic orange emission of Sm^{3+} at 566 nm ($^4G_{5/2} \rightarrow {}^6H_{5/2}$), 602 nm ($^4G_{5/2} \rightarrow {}^6H_{7/2}$) and 653 nm ($^4G_{5/2} \rightarrow {}^6H_{9/2}$) can be observed from the emission spectrum of $GdVO_4$:Sm^{3+} (Fig. 7B, right). Obviously, the strong emission of Sm^{3+} is also due to an energy transfer from $VO_4{}^{3-}$ group to Sm^{3+} ion in $GdVO_4$:Sm^{3+} phosphor. For $GdVO_4$:Dy^{3+}, as indicated in Fig. 7B, left, a strong and broad band ranging 250 nm to 350 nm associated with the absorption of $VO_4{}^{3-}$ can be detected, which is similar to the $GdVO_4$:Eu^{3+} and $GdVO_4$:Sm^{3+} samples. The emission spectrum of $GdVO_4$:Dy^{3+} (Fig. 7B, right) is composed of two

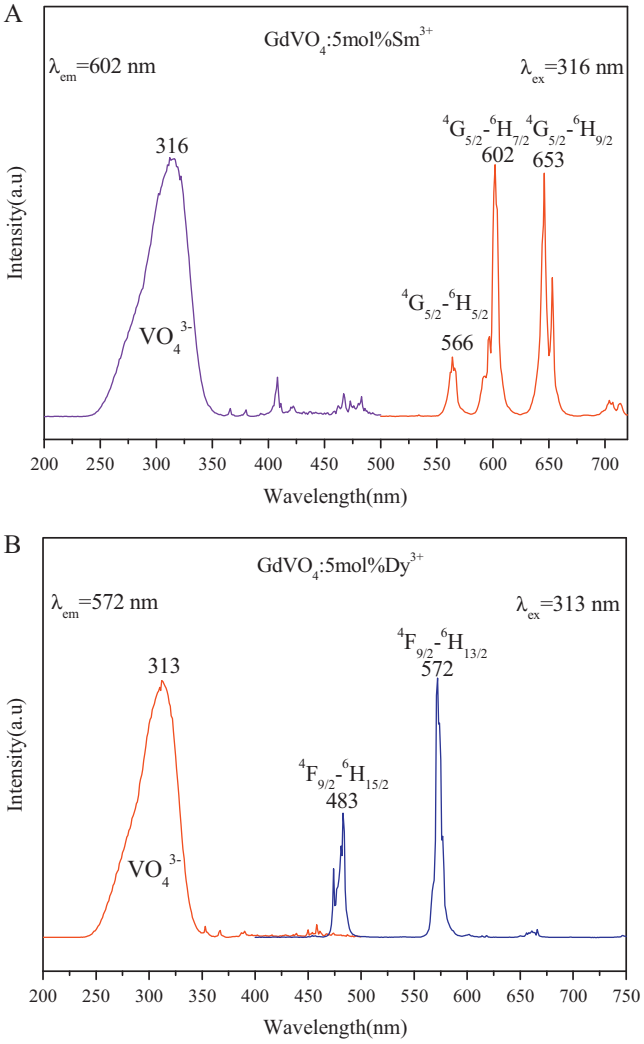

Fig. 7. Excitation and emission spectra of $GdVO_4$:Ln^{3+} (Ln = Sm, Dy) synthesized at 180 °C for 24 h with pH value of 7.2.

characteristic emission peaks of Dy^{3+} upon excitation at 313 nm. The emissions at 483 and 572 nm are associated with the typical transitions from the $^4F_{9/2}$ level to $^6H_{15/2}$ and $^6H_{13/2}$ respectively. The intensity of its yellow emission (572 nm) is stronger than that of the blue emission (483 nm) because the Dy^{3+} ions are located at the site with a D_{2d} symmetry without an inverse center in the host of $GdVO_4$. From the above results and analysis, it is known that the whole excitation and emission process of $GdVO_4$:Ln^{3+} (Ln = Eu, Sm, Dy) under UV radiation include three major steps. The first is the absorption of UV radiation by $VO_4{}^{3-}$ groups. The second is the excited energy is transferred to Ln^{3+} after a thermally activated energy migration through the vanadate sublattice. The last one is the de-excitation process of excited Ln^{3+} ions, emitting strong various colors light [6].

In order to clarify the concentration quenching behavior, the influence of rare earth ions (Eu^{3+}, Sm^{3+}, Dy^{3+}) doping concentration on the photoluminescence emission intensity of $Gd_{(1-x)}VO_4$:xLn^{3+} was investigated and shown in Fig. 8a–c, respectively. It can be seen that the PL intensities of Ln^{3+} doped $GdVO_4$ increase with the increase of rare earth ions doping concentrations, then decrease with further increase of doping concentrations due to the concentration quenching effect [3,5,26,33,35]. Optimal doping appears at a specific concentration. The optimum doping concentrations for

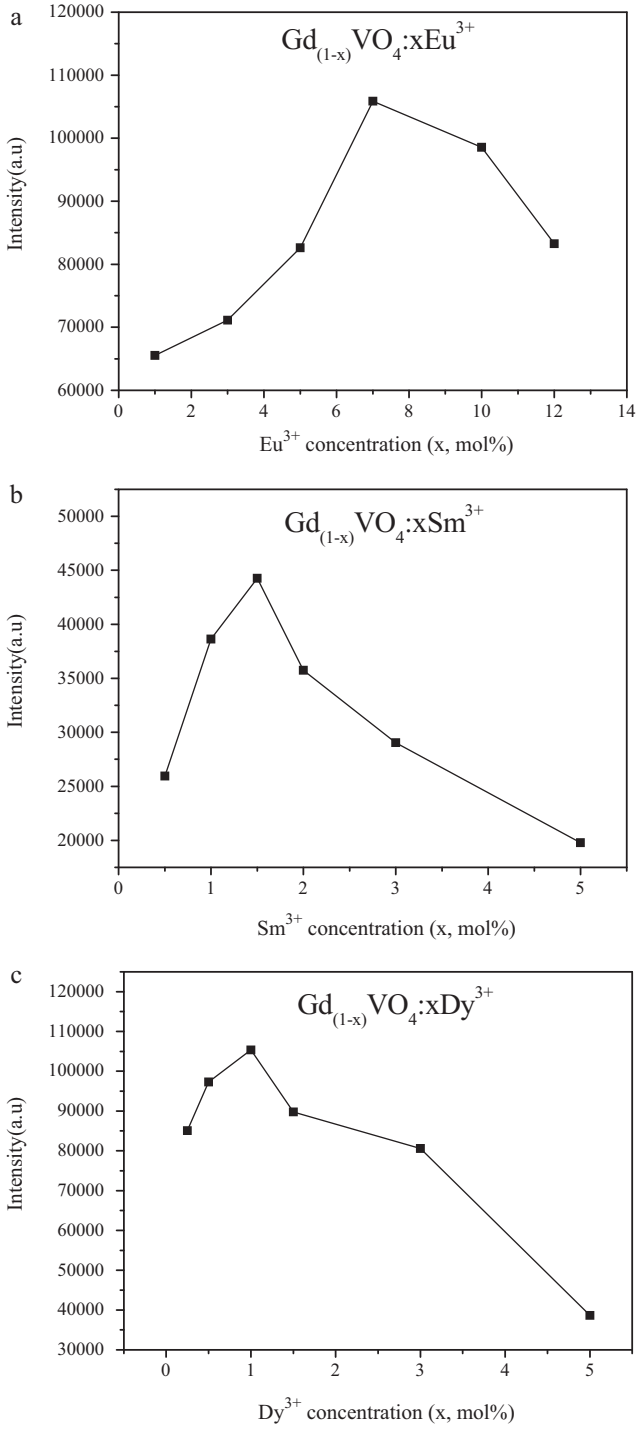

Fig. 8. The photoluminescence emission intensities of $GdVO_4:Ln^{3+}$ (Ln = Eu, Sm, Dy) with different doping concentration.

Eu^{3+}, Sm^{3+} and Dy^{3+} are about 7 mol%, 1.5 mol% and 1 mol%, respectively in the $GdVO_4$ host. After a series of optimization process including adjust pH values, calcination process and change rare ions doping concentration, the photoluminescence quantum yield (QY) for the as-obtained phosphors was performed by Edinburgh FLS920 fluorescence spectrometer with integrated sphere. The quantum yields for the $Gd_{0.93}VO_4:0.07Eu^{3+}$, $Gd_{0.985}VO_4:0.015Sm^{3+}$ and $Gd_{0.99}VO_4:0.01Dy^{3+}$ prepared at pH 11.1 and annealed at 700 °C for 2 h are 64%, 30% and 34% under the excitation of 313 nm, respectively.

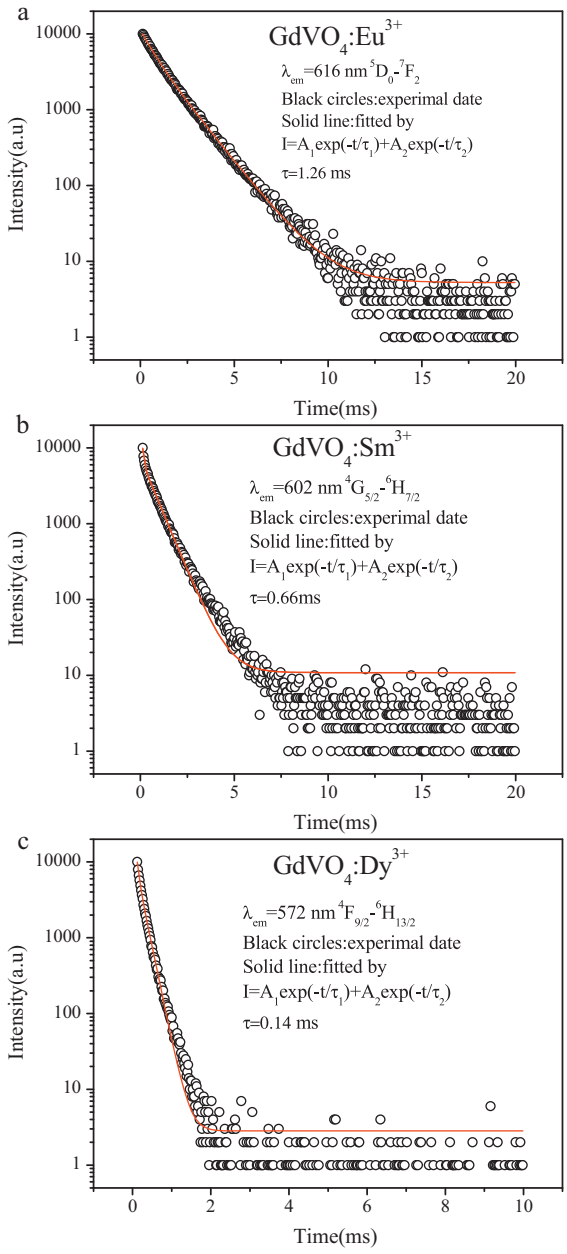

Fig. 9. The luminescence decay curves of $GdVO_4:Eu^{3+}$ (a), $GdVO_4:Sm^{3+}$ (b) and $GdVO_4:Dy^{3+}$ (c) samples prepared at 180 °C for 24 h with pH value of 7.2.

The luminescence decay curves of the $GdVO_4:Eu^{3+}$, $GdVO_4:Sm^{3+}$ and $GdVO_4:Dy^{3+}$ samples are shown in Fig. 9A–C respectively. All these luminescence decay curves of Eu^{3+} (616 nm $^5D_0$–$^7F_2$), Sm^{3+} (602 nm $^4G_{5/2}$–$^6H_{7/2}$) and Dy^{3+} (572 nm $^4F_{9/2}$–$^6H_{13/2}$) in $GdVO_4$ host can all be fitted to a double-exponential functions as $I = A_1 \exp(-t/\tau_1) + A_2 \exp(-t/\tau_2)$, in which τ_1 and τ_2 are the fast and slow components of the luminescent lifetimes, and A_1 and A_2 are the fitting parameters. According to the formula $\tau = (A_1\tau_1^2 + A_2\tau_2^2)/(A_1\tau_1 + A_2\tau_2)$ [5,7,8,27,36,37], the average lifetimes of Eu^{3+}, Sm^{3+} and Dy^{3+} ions in $GdVO_4$ host lattices are determined to be 1.26, 0.66 and 0.14 ms respectively, which are in the same order of magnitude compared with $YVO_4:Ln^{3+}$ (Ln = Eu, Sm, Dy) phosphors as reported in Refs. [7,8]. It is well known that the decay curve depends on the number of luminescence centers, energy transfer, defects and impurities. Generally speaking, if there is one kind of luminescent center in the phosphors, the decay curves can be fit to single exponential function. Two kinds of luminescent

centers or more will lead to a multi-exponential behavior [7,8,38], and the main reasons of the decay curve fitted by single exponential or multi exponential function were discussed and summarized in Ref. [33]. In this case, Ln^{3+} ions occupy the sites of the Gd^{3+} ions with the D_{2d} symmetry in the $GdVO_4$:Ln^{3+} crystals, indicating that only one luminescent center exists. So the multi-exponential behavior may be ascribed to the absorbed impurities which lead to the defects and the quenching centers [7,8]. It is found that in this case, the average lifetimes of Eu^{3+} ions in the $GdVO_4$ host are longer in comparison with 0.552 ms [5], 0.721 ms [18], 0.31 ms [20], 0.719 ms [39] in the $GdVO_4$, and 0.853 ms in core-shell structured spherical SiO_2@$GdVO_4$ phosphors [27], the average lifetimes of Dy^{3+} ions in the $GdVO_4$ is closed to that reported in Refs. [5,20], which was at a range of 0.127–0.152 ms, and the average lifetimes of Sm^{3+} ions in the $GdVO_4$ host are longer than that reported in Refs. [5,20]. The average lifetimes of Eu^{3+}, Dy^{3+}, Sm^{3+} ions differ from the host, such as YVO_4, $YP_xV_{1-x}O_4$ [6–8,40], ZnF_2–WO_3–TeO_2 glasses [41], nanoporous silica spheres [42]. In this case, the average lifetimes of Eu^{3+} ions in the $GdVO_4$ host is closed to that reported in Refs. [7,40–42]. It is well known that the luminescent lifetime of rare earth ion is influenced by the structure of the host, the rare earth located sites (on the surface or bulk) of the host, defect and impurity [8,18,43]. The defect and impurity may act as quenching center, and reduced luminescent lifetime. In this case, longer lifetime may be due to the better crystallization and less defects, which reduces the non-radiative probability and results in the longer lifetimes. The related mechanism should be further investigated.

4. Conclusions

In summary, $GdVO_4$:Ln^{3+} (Ln = Eu, Sm, Dy) phosphors were successfully synthesized by a simple hydrothermal method using $NaVO_3$ as vanadium source. The XRD results show that the pure $GdVO_4$ can be obtained under the current hydrothermal condition (180 °C for 24 h) with different pH values. The pH values of the solution play an important role in the formation of the $GdVO_4$:Eu^{3+} products with different morphologies and particle sizes. The PL measurement reveals that photoluminescence properties of the $GdVO_4$:Eu^{3+} depend on the morphology and the $GdVO_4$:Ln^{3+} (Ln = Eu, Sm, Dy) phosphors show strong red, orange and yellow emission respectively under ultraviolet excitation. The photoluminescence properties of as-prepared samples depended on annealing temperature and ions doping concentration. The luminescence decay curves of all the samples can fit well into a double-exponential function and the lifetimes of the Eu^{3+}-, Sm^{3+}- and Dy^{3+}-doped $GdVO_4$ host are determined to be 1.26, 0.66 and 0.14 ms respectively.

Acknowledgements

The authors acknowledge the joint support of the National High Technology Research and Development Program of China (863 Program) (No. 2009AA03Z217), the Major Research Plan of National Natural Science Foundation of China (No. 90922028), the National Natural Science Foundation of China (No. 50842027), Fujian Natural Science Foundation (No. 2010J01289) and Scientific Research Foundation of Overseas Chinese Affairs Office of State Council, China (No. 07QZR06).

References

[1] V. Natarajan, A.R. Dhobale, C.H. Lu, J. Lumin. 129 (2009) 290.
[2] J.W. Chung, H.K. Yang, B.K. Moon, B.C. Choi, J.H. Jeong, J.S. Bae, K.H. Kim, Curr. Appl. Phys. 9 (2009) S222.
[3] N.S. Singh, R.S. Ningthoujam, S.D. Singh, B. Viswanadh, N. Manoj, R.K. Vasta, J. Lumin. 130 (2010) 2452.
[4] N. Wang, W. Chen, Q.F. Zhang, Y. Dai, Mater. Lett. 62 (2008) 109.
[5] X. Li, M. Yu, Z.Y. Hou, G.G. Li, P.A. Ma, W.X. Wang, Z.Y. Cheng, J. Lin, J. Solid State Chem. 184 (2011) 141.
[6] Z.H. Xu, X.J. Kang, C.X. Li, Z.Y. Hou, C.M. Zhang, D.M. Yang, G.G. Li, J. Lin, Inorg. Chem. 49 (2010) 6706.
[7] G. Jia, Y.H. Song, M. Yang, Y.J. Huang, L.H. Zhang, H.P. You, Opt. Mater. 31 (2009) 1032.
[8] F. He, P.P. Yang, N. Niu, W.X. Wang, S.L. Gai, D. Wang, J. Lin, J. Colloids Interface Sci. 343 (2010) 71.
[9] M. Yu, J. Lin, Z. Wang, J. Fu, S. Wang, H.J. Zhang, Y.C. Han, Chem. Mater. 14 (2002) 2224.
[10] J.Y. Choe, D. Ravichandran, S.M. Blomquist, D.C. Morton, K.W. Kirchner, M.H. Ervin, U. Lee, Appl. Phys. Lett. 78 (2001) 3800.
[11] A.K. Levine, F.C. Palilla, Electrochem. Technol. 4 (1966) 16.
[12] S. Neeraj, N. Kijima, A.K. Cheetham, Solid State Commun. 131 (2004) 65.
[13] K.S. Sohn, I.W. Zeon, H. Chang, S.K. Lee, H.D. Park, Chem. Mater. 14 (2002) 2140.
[14] J.S. Bae, S.S. Park, T.E. Hong, J.P. Kim, J.H. Yoon, E.D. Jeong, M.S. Won, J.H. Jeong, Curr. Appl. Phys. 9 (2009) S241.
[15] X.Q. Su, B. Yan, H.H. Huang, J. Alloys Compd. 399 (2005) 251.
[16] W. Xu, Y. Wang, X. Bai, B. Dong, Q. Liu, J.S. Chen, H.W. Song, J. Phys. Chem. C 114 (2010) 14018.
[17] L.M. Chen, Y.N. Liu, K.L. Huang, Mater. Res. Bull. 41 (2006) 158.
[18] Y.H. Zheng, H.P. You, G. Jia, K. Liu, Y.H. Song, M. Yang, H.J. Zhang, Cryst. Growth Des. 9 (2009) 5101.
[19] M. Gu, Q. Lin, S.P. Mao, D.L. Mao, C.K. Chang, Cryst. Growth Des. 8 (2008) 1422.
[20] Y. Su, L. Li, G. Li, J. Liu, X. Chen, W. Hu, G. Liu, J. Nanosci. Nanotechnol. 10 (2010) 1877.
[21] B. Yan, J.F. Gu, J. Exp. Nanosci. 4 (2009) 301.
[22] C.C. Zhang, Z.M. Zhang, R.C. Dai, Z.P. Wang, J.W. Zhang, Z.J. Ding, J. Phys. Chem. C 114 (2010) 18279.
[23] Y.H. Wang, Y.Y. Zuo, H. Gao, Mater. Res. Bull. 41 (2006) 2147.
[24] A. Newport, J. Silver, A. Vecht, J. Electrochem. Soc. 147 (2000) 3944.
[25] B. Yan, X.Q. Su, Opt. Mater. 29 (2007) 1866.
[26] Y.H. Zhou, J. Lin, Opt. Mater. 27 (2005) 1426.
[27] G.Z. Li, Z.L. Wang, M. Yu, Z.W. Quan, J. Lin, J. Solid State Chem. 179 (2006) 2698.
[28] R. Calderón-Villajos, C. Zaldo, C. Cascales, Phys. Proc. 8 (2010) 109.
[29] M. Yu, J. Lin, J. Fang, Chem. Mater. 17 (2005) 1783.
[30] A. Bao, H. Lai, Y.M. Yang, W.W. Xu, C.H. Tao, H. Zhang, H. Yang, J. Cryst. Growth 310 (2008) 4394.
[31] J. Wang, Y.H. Xu, M. Hojamberdiev, G.Q. Zhu, J. Alloys Compd. 487 (2009) 358.
[32] J. Wang, Y.H. Xu, M. Hojamberdiev, J.H. Peng, G.Q. Zhu, Mater. Sci. Eng. B 156 (2009) 42.
[33] N. Shanta Singh, R.S. Ningthoujam, M. Niraj Luwang, S. Dorendrajit Singh, R.K. Vatsa, Chem. Phys. Lett. 480 (2009) 237.
[34] S. Choi, Y.-M. Moon, H.-K. Jung, J. Lumin. 130 (2010) 549.
[35] Y.H. Zhou, J. Lin, J. Alloys Compd. 408–412 (2006) 856.
[36] H. Wang, M. Yu, C.K. Lin, J. Lin, J. Colloids Interface Sci. 300 (2006) 176.
[37] M. Yu, J. Lin, J. Fang, Chem. Mater. 17 (2005) 1738.
[38] X.M. Lin, J. Lin, Solid State Sci. 11 (2009) 2030.
[39] H.K. Yang, B.K. Moon, B.C. Choi, J.H. Jeong, K.H. Kim, CryEngComm 13 (2011) 4723.
[40] Y. Jin, C. Li, Z. Xu, Z. Cheng, W. Wang, G. Li, J. Lin, Mater. Chem. Phys. 129 (2011) 418.
[41] Y. Gandhi, I.V. Kityk, M.G. Brik, P. Raghava Rao, N. Veeraiah, J. Alloys Compd. 508 (2006) 278.
[42] M. Tagaya, T. Ikoma, T. Yoshioka, S. Motozuka, Z. Xu, F. Minami, J. Tanaka, J. Colloids Interface Sci. 363 (2011) 456.
[43] V. Sudarsan, F. Veggel, R. Herring, M. Raudsepp, J. Mater. Chem. 15 (2005) 1332.